

# Baryons in the large $N$ limit of the massive two-dimensional Nambu–Jona-Lasinio model

Christian Boehmer, Felix Karbstein, and Michael Thies\*

*Institut für Theoretische Physik III, Universität Erlangen-Nürnberg, D-91058 Erlangen, Germany*

(Dated: November 27, 2018)

Baryons in the massive Nambu–Jona-Lasinio model in 1+1 dimensions (the massive chiral Gross-Neveu model) are studied in the limit of an infinite number of flavors. The baryon mass is evaluated for a wide range of bare fermion masses and filling fractions, combining analytical asymptotic expansions with a full numerical Hartree-Fock calculation.

PACS numbers: 11.10.-z, 11.10.Kk, 11.10.St

## I. INTRODUCTION

Since the seminal paper by Gross and Neveu in 1974 [1], field theoretic models of fermions in 1+1 dimensions with (broken or unbroken) chiral symmetry have turned out to be quite useful. In view of a long list of applications in particle, condensed matter and mathematical physics, it is surprising that after more than three decades the basic solution of these models is still incomplete, even in the tractable limit of an infinite number of flavors  $N$ . A few years ago it has been realized that the alleged phase diagram of Gross-Neveu (GN) models in the temperature ( $T$ ) versus chemical potential ( $\mu$ ) plane [2, 3] was inconsistent with the known baryon spectrum. In the standard GN model with scalar-scalar interaction, this problem has been solved in the meantime with the construction of a soliton crystal phase (see [4] and references therein) built out of Dashen-Hasslacher-Neveu baryons [5]. However there are still large gaps in our understanding of the model with continuous chiral symmetry, i.e., the Nambu–Jona-Lasinio model [6] in two dimensions (NJL<sub>2</sub>). In the chiral limit, it is known that solitonic baryons and soliton crystals do exist here as well, although their properties are quite distinct from those of the standard GN model [7]. In particular, induced fermion number plays an important role in the NJL<sub>2</sub> model [8]. By contrast, in the massive NJL<sub>2</sub> model, very little is known yet about either baryons or the phase diagram. We are aware of only two works addressing the issue of baryons at finite bare fermion mass. Salcedo et al. [9] use an elegant variational ansatz to reduce the problem to the sine-Gordon kink, both in the 't Hooft model [10] and the NJL<sub>2</sub> model, and point out the close relationship to the Skyrme picture in higher dimensions [11]. In Ref. [12] the sine-Gordon equation was subsequently identified as the first term of a systematic chiral expansion and higher order corrections were determined with the help of derivative expansion techniques. In the present work, we try to further improve this situation by

constructing baryons in the (large  $N$ ) NJL<sub>2</sub> model for arbitrary bare fermion mass, using a combination of analytical and numerical methods. Our ultimate goal is the phase diagram of the model which will be discussed elsewhere. Like in the GN model, we expect the baryon mass to play the role of the critical chemical potential where a soliton crystal phase sets in at zero temperature. Aside from their importance for the phase diagram, baryons in the massive NJL<sub>2</sub> model are also of interest in their own right. By varying the bare fermion mass, we have the unique possibility to interpolate between the Skyrme picture characteristic for the chiral limit and the non-relativistic valence picture expected to hold in the heavy fermion limit.

Let us now pose the baryon problem at large  $N$  in a more precise fashion. The Lagrangian of the (massive) NJL<sub>2</sub> model reads

$$\mathcal{L} = \bar{\psi}(i\partial - m_0)\psi + \frac{g^2}{2} [(\bar{\psi}\psi)^2 + (\bar{\psi}i\gamma_5\psi)^2] \quad (1)$$

where flavor indices are suppressed as usual, i.e.,  $\bar{\psi}\psi = \sum_{k=1}^N \bar{\psi}_k\psi_k$  etc. In the large  $N$  limit the Hartree-Fock (HF) approximation [13], or, equivalently, the stationary phase approximation to the functional integral [5], become exact. The Dirac-HF equation

$$(-\gamma_5 i\partial_x + \gamma^0 S(x) + i\gamma^1 P(x))\psi_\alpha = E_\alpha\psi_\alpha \quad (2)$$

for the single particle orbital  $\alpha$  has to be solved simultaneously with the self-consistency conditions

$$\begin{aligned} S &= m_0 - Ng^2 \sum_{\alpha}^{\text{occ}} \bar{\psi}_\alpha\psi_\alpha, \\ P &= -Ng^2 \sum_{\alpha}^{\text{occ}} \bar{\psi}_\alpha i\gamma_5\psi_\alpha. \end{aligned} \quad (3)$$

The HF energy

$$E_{\text{HF}} = \sum_{\alpha}^{\text{occ}} E_\alpha + \frac{1}{2g^2} \int dx [(S - m_0)^2 + P^2] \quad (4)$$

comprises the sum over single particle energies of all occupied states (including the Dirac sea) and the standard

\*Electronic addresses:  
christian.boehmer,felix,thies@theorie3.physik.uni-erlangen.de

correction for double counting of the potential energy. The vacuum problem is a special case of Eqs. (2-4) where  $S = m$  (the physical fermion mass),  $P = 0$ , and all negative energy states are filled. Self-consistency then yields the gap equation (in units where  $m = 1$ , and using the ultraviolet (UV) cutoff  $\Lambda/2$  [12])

$$\frac{\pi}{Ng^2} = \gamma + \ln \Lambda. \quad (5)$$

Here we have introduced the ‘‘confinement parameter’’  $\gamma$  [14, 15],

$$\gamma = m_0 \ln \Lambda, \quad (6)$$

where the name (borrowed from condensed matter physics) refers to confinement of kink and antikink, not of the elementary fermions. Trading the bare parameters ( $g^2, m_0$ ) for the physical parameters ( $m = 1, \gamma$ ) with the help of Eqs. (5,6) is all that is needed to renormalize the model and eliminate divergences in the baryon problem. Baryons in the HF approach are characterized by  $x$ -dependent potentials  $S(x), P(x)$  and one (partially or fully) occupied extra level as compared to the vacuum. The observables of most interest to us are the baryon mass, defined as the difference in HF energies between baryon state and vacuum, the self-consistent potentials  $S, P$  and the fermion density.

We shall use both analytical and numerical methods, depending on the parameters. The paper is organized accordingly. In Sec. II, we remind the reader of the derivative expansion and collect the results relevant for the vicinity of the chiral limit. In Sec. III we apply a recently developed effective field theory for the valence level [16] to get complementary analytical insight into the non-relativistic regime. The full numerical solution of the HF problem including the Dirac sea is presented in Sec. IV. Sec. V contains a short summary and our conclusions.

## II. DERIVATIVE EXPANSION

In general the HF problem as defined through Eqs. (2,3) is rather involved. This raises the question whether one can bypass its full solution, at least in some regions of parameter space. Near the chiral limit, the potentials  $S, P$  become very smooth. It is then possible to ‘‘integrate out’’ the fermions approximately, using the derivative expansion technique, see e.g. Refs. [17, 18]. This method presupposes full occupation of each level with  $N$  fermions and is inapplicable for partially occupied levels. It results in a purely bosonic effective field theory for the complex scalar field  $\Phi = S - iP$  which, in the large  $N$  limit, can be treated classically. Hence, one gets direct access to the HF potential without need to solve the Dirac-HF equation self-consistently. The leading order reproduces the sine-Gordon approach of Ref. [9]. In Refs. [12, 19] this program was carried through to rather

high order in the derivative expansion, yielding a systematic expansion in the ratio of pion mass to physical fermion mass. The field  $\Phi$  was computed in polar coordinates,

$$\Phi = (1 + \lambda)e^{2i\chi}, \quad (7)$$

with  $\lambda, \chi$  expressed in terms of the pion mass  $m_\pi$  and the spatial variable  $\xi = m_\pi x$ . For the present purpose, we express everything in terms of the confinement parameter  $\gamma$ , using the (approximate) relationship

$$m_\pi = 2\sqrt{\gamma} \left( 1 - \frac{1}{3}\gamma + \frac{11}{90}\gamma^2 - \frac{5}{126}\gamma^3 \right). \quad (8)$$

To this order in  $\gamma$ , the baryon mass is given by

$$M_B = \frac{4\sqrt{\gamma}N}{\pi} \left( 1 - \frac{4}{9}\gamma + \frac{9}{50}\gamma^2 - \frac{101}{735}\gamma^3 \right), \quad (9)$$

whereas the result for the potentials translates into

$$\begin{aligned} S &= 1 - \frac{2}{\cosh^2 \xi} + \frac{2}{\cosh^4 \xi} \gamma \\ &\quad - \frac{2}{9} \left( \frac{20}{\cosh^2 \xi} - \frac{55}{\cosh^4 \xi} + \frac{41}{\cosh^6 \xi} \right) \gamma^2, \\ P &= \frac{2 \sinh \xi}{\cosh^2 \xi} \left[ 1 - \frac{1}{2} \left( 1 + \frac{2}{\cosh^2 \xi} \right) \gamma \right. \\ &\quad \left. + \frac{1}{72} \left( 47 - \frac{276}{\cosh^2 \xi} + \frac{328}{\cosh^4 \xi} \right) \gamma^2 \right]. \end{aligned} \quad (10)$$

In the vicinity of the chiral limit, fermion number is induced by the topologically non-trivial field  $\Phi$  and thus only resides in the negative energy states. For the fermion number divided by  $N$  (‘‘baryon number’’), the derivative expansion yields

$$B = \int dx \left( \frac{\chi'}{\pi} \right) = \frac{1}{\pi} [\chi(\infty) - \chi(-\infty)], \quad (11)$$

relating baryon number to chiral U(1) winding number of the field  $\Phi$ , much like in the Skyrme model. One cannot conclude from this result that the induced fermion density is given by  $\chi'/\pi$  though. As discussed in Ref. [8], the fermion density can be determined from the equation for the partially conserved axial current (PCAC),

$$\partial_\mu j_5^\mu = 2m_0 \bar{\psi} i \gamma_5 \psi. \quad (12)$$

Taking the expectation value of Eq. (12) in the baryon state, using the relationship  $j_5^\mu = \epsilon^{\mu\nu} j_\nu$  (valid in two dimensions) and integrating over  $x$ , one finds the fermion density per flavor

$$\rho = -\frac{2\gamma}{\pi} \int_{-\infty}^x dx' P(x'). \quad (13)$$

An expansion in  $\gamma$  then yields in the present case

$$\begin{aligned} \rho &= \frac{2\sqrt{\gamma}}{\pi \cosh \xi} \left[ 1 - \frac{1}{6} \left( 1 + \frac{2}{\cosh^2 \xi} \right) \gamma \right. \\ &\quad \left. + \frac{1}{360} \left( 171 - \frac{500}{\cosh^2 \xi} + \frac{328}{\cosh^4 \xi} \right) \gamma^2 \right]. \end{aligned} \quad (14)$$

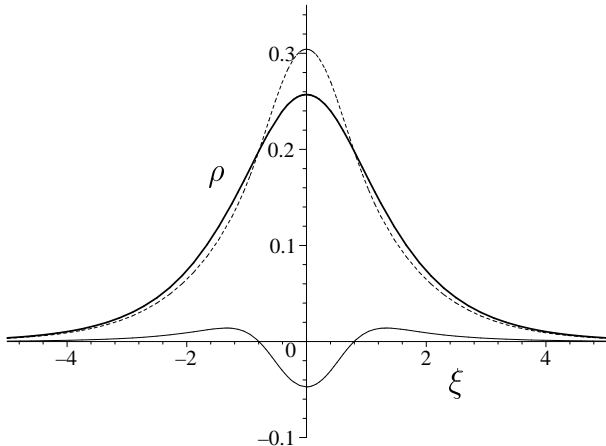


FIG. 1: Thick solid line: induced fermion density (14), dashed line: leading order term  $\chi'/\pi$ , thin line: difference, according to derivative expansion ( $\gamma = 0.2$ ).

Judging from the convergence properties of the series in  $\gamma$ , we expect expressions (8-14) to be quantitatively reliable up to  $\gamma \approx 0.2$ .

Let us use these results to exhibit some differences between baryons in massive GN and NJL<sub>2</sub> models, respectively. First of all, in the GN model, there is no induced, but only valence fermion density. The negative energy states cancel exactly when taking the difference between the fermion density of the baryon and the vacuum [12]. Turning to the NJL<sub>2</sub> model, the situation is different. In Fig. 1 we illustrate the induced fermion density for the case  $\gamma = 0.2$  and compare it with the naive expectation  $\chi'/\pi$ . The difference integrates to 0, in agreement with Eq. (11). Another pertinent observation is the following. In the GN model, the scalar potential  $S$  is reflectionless for any static solution [4, 20]. This has turned out to be instrumental for the exact, analytical solvability of the baryon problem. We can now easily check whether the same is true for the NJL<sub>2</sub> model, at least in the region of validity of the derivative expansion. By solving the Dirac scattering problem with potential (10), we find that this potential is not transparent, see Fig. 2 for the case  $\gamma = 0.2$ . The transmission coefficient rises from 0 at low energies to 1 at high energies. Similar results are obtained at other values of  $\gamma$ . This is at variance with claims in the literature [21] (see however Ref. [22]) and already indicates that the baryon problem in the NJL<sub>2</sub> model is more challenging than in the GN model.

### III. NO-SEA EFFECTIVE THEORY

Recently, an approximation has been devised which yields analytical insight into the regime where the baryon features one positive energy valence level, while still having smooth HF potentials. The idea is to integrate out the negative energy fermions (i.e., the Dirac sea) and de-

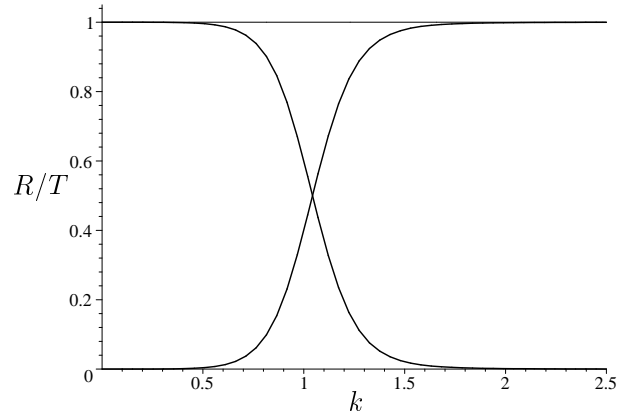


FIG. 2: Reflection coefficient  $R$  (falling curve) and transmission coefficient  $T$  (rising curve) for baryon HF potential (10) versus momentum ( $\gamma = 0.2$ ).

rive an effective theory for the (positive energy) valence fermions only. The HF equation for the baryon then reduces to a single non-linear (and in general non-local) Dirac equation. This is a tremendous simplification as compared to the full relativistic HF problem, although somewhat more involved than the derivative expansion of Sec. II, where the fermions have been integrated out altogether. For the derivation of the effective Lagrangian in the massive NJL<sub>2</sub> model, we refer to Ref. [16]. Here we concentrate on the solution of the non-linear Dirac equation and the determination of the parameter region where the proposed truncation is valid.

We proceed as follows. The effective no-sea Lagrangian consists of a massive free Dirac part and interaction terms descending from the original scalar and pseudoscalar four-fermion interactions. As far as terms involving only scalar interactions are concerned, we keep all contributions in Eq. (39) of Ref. [16]. The terms involving pseudoscalar interactions require one additional approximation. Starting point is the result for the massive NJL<sub>2</sub> model, Eq. (76) of [16], replacing the scalar effective coupling constant  $g_{\text{eff}}^2 = \pi/N$  by the corresponding expression in the massive model (cf. Eq. (72) of [16]). If we insist on an analytical solution as we do in this section, we are only able to handle the case in which the non-locality due to one-pion exchange is of short range. We therefore assume that the mass term  $m_\pi^2 = 4\gamma$  dominates the inverse pion propagator and expand in the remaining two terms as follows,

$$\frac{2\pi}{N} \bar{\psi} i\gamma_5 \psi \frac{1}{\square + m_\pi^2 - \frac{4\pi}{N(1+\gamma)} \bar{\psi}\psi} \bar{\psi} i\gamma_5 \psi \approx \quad (15)$$

$$\frac{2\pi}{N} \bar{\psi} i\gamma_5 \psi \frac{1}{m_\pi^2} \left( 1 - \frac{\square}{m_\pi^2} + \frac{4\pi \bar{\psi}\psi}{Nm_\pi^2(1+\gamma)} \right) \bar{\psi} i\gamma_5 \psi.$$

The result is added to the GN model effective Lagrangian. At this stage it is difficult to predict the precise range of applicability of the approximation due to the unavoidable issue of self-consistency. We will return to this

question once we have solved the non-linear Dirac-HF

equation. The final effective Lagrangian reads ( $m = 1$ )

$$\begin{aligned} \mathcal{L}_{\text{eff}} = & \bar{\psi}(i\partial - 1)\psi + \frac{\pi}{2N} \frac{1}{(1+\gamma)} (\bar{\psi}\psi)^2 - \frac{\pi}{24N} \frac{1}{(1+\gamma)^2} (\square\bar{\psi}\psi)(\bar{\psi}\psi) + \frac{\pi^2}{6N^2} \frac{1}{(1+\gamma)^3} (\bar{\psi}\psi)^3 \\ & + \frac{11\pi}{1440N} \frac{(1+6\gamma/11)}{(1+\gamma)^3} (\square^2\bar{\psi}\psi)(\bar{\psi}\psi) - \frac{\pi^2}{12N^2} \frac{(1+\gamma/2)}{(1+\gamma)^4} (\square\bar{\psi}\psi)(\bar{\psi}\psi)^2 + \frac{\pi^3}{6N^3} \frac{(1+\gamma/4)}{(1+\gamma)^5} (\bar{\psi}\psi)^4 \\ & + \frac{\pi}{2N\gamma} (\bar{\psi}i\gamma_5\psi)^2 - \frac{\pi}{8N\gamma^2} (\square\bar{\psi}i\gamma_5\psi)(\bar{\psi}i\gamma_5\psi) + \frac{\pi^2}{2N^2\gamma^2} \frac{1}{(1+\gamma)} (\bar{\psi}i\gamma_5\psi)^2 (\bar{\psi}\psi). \end{aligned} \quad (16)$$

By construction, it is to be used in the positive energy sector only, since the effects of the negative energy states are already encoded in the Lagrangian. For a single baryon, the ensuing Euler-Lagrange equation is the non-linear Dirac equation for the (normalized) valence spinor,

$$(-\gamma_5 i \partial_x + \gamma^0 S + i\gamma^1 P) \psi_0 = E_0 \psi_0, \quad \int dx \psi_0^\dagger \psi_0 = 1. \quad (17)$$

Assuming the valence level to be occupied with filling fraction  $\nu = n/N$  (where  $n$  is the valence fermion number) and using  $\eta = \pi\nu$  for ease of notation (all  $\pi$ 's disappear), the scalar and pseudoscalar potentials are expressed self-consistently as ( $' = \partial_x$ )

$$\begin{aligned} S = & 1 - \frac{\eta s_0}{(1+\gamma)} - \frac{\eta s_0''}{12(1+\gamma)^2} - \frac{\eta^2 s_0'^2}{2(1+\gamma)^3} \\ & - \frac{11\eta(1+6\gamma/11)s_0^{IV}}{720(1+\gamma)^3} - \frac{\eta^2(1+\gamma/2)}{6(1+\gamma)^4} (2s_0''s_0 + (s_0')^2) \\ & - \frac{2\eta^3(1+\gamma/4)s_0^3}{3(1+\gamma)^5} - \frac{\eta^2 p_0^2}{2\gamma^2(1+\gamma)}, \\ P = & -\frac{\eta p_0}{\gamma} - \frac{\eta p_0''}{4\gamma^2} - \frac{\eta^2 p_0 s_0}{\gamma^2(1+\gamma)} \end{aligned} \quad (18)$$

through scalar ( $s_0$ ) and pseudoscalar ( $p_0$ ) valence level condensates

$$s_0 = \bar{\psi}_0 \psi_0, \quad p_0 = \bar{\psi}_0 i\gamma_5 \psi_0. \quad (19)$$

It seems hopeless to solve the complicated non-linear Dirac equation (17-19) in closed analytical form. However, since the Lagrangian (16) is an approximate one, it is sufficient to solve the equation perturbatively in some formal expansion parameter. We choose to expand in  $\nu$  and postpone till later the discussion of the validity of the truncation scheme. In order to solve the Dirac equation, we then find that we first have to solve a simple non-linear differential equation, followed by a sequence of inhomogeneous, linear differential equations. The lengthy analytical computations can be done conveniently with computer algebra (we used MAPLE), therefore we skip the details and record only the final results. The baryon mass (computed from the classical field energy) has the

following power series expansion in  $\eta = \pi\nu$ ,

$$\begin{aligned} \pi \frac{M_B}{N} = & \eta - \frac{\eta^3}{24(1+\gamma)^2} + \frac{(\gamma^2 - 15\gamma - 8)\eta^5}{1920\gamma(1+\gamma)^5} \\ & - \frac{(\gamma^4 - 302\gamma^3 + 265\gamma^2 + 376\gamma + 88)\eta^7}{322560\gamma^2(1+\gamma)^8}. \end{aligned} \quad (20)$$

The energy  $E_0$  of the valence level is closely related to  $M_B$ . According to standard HF theory, the single particle energy can be interpreted as removal energy of a fermion, or equivalently

$$E_0 = \frac{\partial M_B}{\partial n}. \quad (21)$$

This is indeed what we find in the calculation, so that there is no need to spell out  $E_0$ . Next we turn to the HF potentials (18) derived from the self-consistent valence level spinor  $\psi_0$ . For the scalar and pseudoscalar potentials, we obtain

$$\begin{aligned} S = & 1 + \frac{s_{22}}{\cosh^2 \xi} \eta^2 + \left( \frac{s_{42}}{\cosh^2 \xi} + \frac{s_{44}}{\cosh^4 \xi} \right) \eta^4 \\ & + \left( \frac{s_{62}}{\cosh^2 \xi} + \frac{s_{64}}{\cosh^4 \xi} + \frac{s_{66}}{\cosh^6 \xi} \right) \eta^6 \\ P = & \left[ \frac{p_{33}}{\cosh^3 \xi} \eta^3 + \left( \frac{p_{53}}{\cosh^3 \xi} + \frac{p_{55}}{\cosh^5 \xi} \right) \eta^5 \right] \sinh \xi \end{aligned} \quad (22)$$

with  $\gamma$ -dependent coefficients  $s_{nm}, p_{nm}$  relegated to the appendix in order to keep the paper readable (the subscripts  $n, m$  denote the powers of  $\eta$  and  $1/\cosh \xi$ , respectively). The spatial variable  $\xi = yx$  in Eq. (22) involves a scale factor

$$\begin{aligned} y = & \frac{\eta}{2(1+\gamma)} - \frac{(\gamma^2 - 3\gamma - 2)\eta^3}{48\gamma(1+\gamma)^4} \\ & + \frac{(3\gamma^4 - 226\gamma^3 - 65\gamma^2 + 68\gamma + 24)\eta^5}{11520\gamma^2(1+\gamma)^7}. \end{aligned} \quad (23)$$

One verifies that it is related to the single particle energy  $E_0$  via

$$E_0 = \sqrt{1 - y^2}. \quad (24)$$

This last relation can be understood in physics terms as follows. Asymptotically, the valence wave function falls off exponentially with the  $\kappa$  value (imaginary momentum) of the bound state. Due to self-consistency, the same parameter will govern the asymptotic exponential decay of the potentials in a no-sea HF calculation. This is exactly what Eq. (24), together with the shape of the potentials  $S$  and  $P$ , guarantees.

We note in passing that the asymptotic expansions for the scalar potential  $S$  at small  $\gamma$ , Eq. (10), and at large  $\gamma$  or small  $\nu$ , Eq. (22), have the same functional form. This is not true for the pseudoscalar potential  $P$  where Eq. (10) involves even, Eq. (22) odd powers of  $1/\cosh\xi$ .

We have tested the above results in two different ways. If we switch off the pseudoscalar coupling, we can carry out the same calculation for the massive GN model and reproduce the well-known exact results to the expected accuracy. A more specific test of the NJL<sub>2</sub> model calculation is provided by the divergence of the axial current implying [8]

$$\partial_x \rho = -\frac{2\gamma}{\pi} P. \quad (25)$$

Here  $\rho$  denotes the fermion density per flavor consisting of the valence density and the induced part from the Dirac sea ( $n = \nu N$ ),

$$\rho = \nu \psi_0^\dagger \psi_0 - \frac{1}{2\pi} \partial_x P. \quad (26)$$

Eqs. (25,26) yield the following non-trivial identity relating the valence fermion density to the pseudoscalar HF potential,

$$\nu \partial_x (\psi_0^\dagger \psi_0) = -\frac{2\gamma}{\pi} P + \frac{1}{2\pi} \partial_x^2 P. \quad (27)$$

In our calculation it is violated at order  $\nu^7$ . For the sake of completeness, let us quote the separate results for the valence fermion density  $\rho_{\text{val}} = \nu \psi_0^\dagger \psi_0$ ,

$$\begin{aligned} \pi \rho_{\text{val}} &= \frac{v_{22}}{\cosh^2 \xi} \eta^2 + \left( \frac{v_{42}}{\cosh^2 \xi} + \frac{v_{44}}{\cosh^4 \xi} \right) \eta^4 \\ &+ \left( \frac{v_{62}}{\cosh^2 \xi} + \frac{v_{64}}{\cosh^4 \xi} + \frac{v_{66}}{\cosh^6 \xi} \right) \eta^6, \end{aligned} \quad (28)$$

and for the induced fermion density  $\rho_{\text{ind}} = -\frac{1}{2\pi} \partial_x P$ ,

$$\begin{aligned} \pi \rho_{\text{ind}} &= \left( \frac{i_{42}}{\cosh^2 \xi} + \frac{i_{44}}{\cosh^4 \xi} \right) \eta^4 \\ &+ \left( \frac{i_{62}}{\cosh^2 \xi} + \frac{i_{64}}{\cosh^4 \xi} + \frac{i_{66}}{\cosh^6 \xi} \right) \eta^6, \end{aligned} \quad (29)$$

where the coefficients can again be found in the appendix.

Let us now discuss the range of validity of our truncation. The most obvious candidate is the regime

$$\gamma \gg 1 \quad (\text{regime I}) \quad (30)$$

and arbitrary  $\nu$ . In this case we can read off from our results that  $\bar{\psi}\psi \sim 1/\gamma$ ,  $\bar{\psi}i\gamma_5\psi \sim 1/\gamma^2$  and  $\square \sim 1/\gamma^2$ . Inspection of the coefficients in  $\mathcal{L}_{\text{eff}}$  then shows that we have kept all terms up to order  $1/\gamma^8$  in an asymptotic expansion for large  $\gamma$ . Since the identity (27) is violated at order  $1/\gamma^7$  we can trust the results (expanded in  $1/\gamma$ ) up to order  $1/\gamma^6$ . By way of example, we note for future reference the asymptotic behavior of  $M_B$  for  $\gamma \rightarrow \infty$  and full occupation of the valence level ( $\nu = 1$ ) complementary to Eq. (9),

$$\begin{aligned} \frac{M_B}{N} &= 1 - \frac{\pi^2}{24\gamma^2} + \frac{\pi^2}{12\gamma^3} - \frac{\pi^2(240 - \pi^2)}{1920\gamma^4} \\ &+ \frac{\pi^2(16 - \pi^2)}{96\gamma^5} - \frac{\pi^2(67200 - 13776\pi^2 + \pi^4)}{322560\gamma^6}. \end{aligned} \quad (31)$$

Another case of interest is weak occupation of the valence level, i.e., taking the formal expansion in  $\nu$  literally. Here,  $\bar{\psi}\psi \sim \nu^2$ ,  $\bar{\psi}i\gamma_5\psi \sim \nu^3$ ,  $\square \sim \nu^2$  and all terms up to order  $\nu^8$  are kept in  $\mathcal{L}_{\text{eff}}$ . A necessary condition for this to be valid is  $\nu \ll 1$ . Due to the expansion of the propagator in Eq. (15), inverse powers of  $\gamma$  appear in the coefficients, and we have to require in addition  $\nu^2 \ll \gamma$ . In this regime, all terms are then consistently kept and, according to the test based on Eq. (27), the results are trustworthy up to order  $\nu^6$ . This 2nd regime of applicability may be summarized as

$$\nu \ll \min(1, \sqrt{\gamma}) \quad (\text{regime II}). \quad (32)$$

If the condition  $\nu \ll \sqrt{\gamma}$  does not hold, the non-locality of the effective action becomes long range and our approximation breaks down.

We wind up this section with a summary of the analytical results obtained in Secs. II and III. From a practical point of view, it is fairly easy to judge the quality of an effective theory by comparing successive orders in the expansion. This is illustrated in Fig. 3 where we plot the baryon mass (per flavor)  $M_B/N$  as computed from Eqs. (9) and (20) versus  $\nu$  and  $\gamma$ . We only display the result if the highest order correction kept contributes less than 0.002 of the total result (other numerical values for the tolerance would give qualitatively similar plots). This shows clearly that the derivative expansion (curve starting at  $\nu = 1, \gamma = 0$ ) and the no-sea effective theory (tilted surface) are valid in disjoint regions of the diagram, separated by a gap. Needless to say, the no-sea calculation is also valid at higher values of  $\gamma$  not shown here. The structure of the baryons is very different, depending on which asymptotic expansion we look at. Baryons described by the derivative expansion have no filled positive energy level, so that baryon number is entirely due to fermion number induced in the Dirac sea. If on the other hand the no-sea effective theory applies, there has to be a positive energy valence level, and the valence fermion density dominates over the induced one, cf. the powers of  $\eta$  in Eqs. (28,29). Our formulae also show that in the limit of large  $\gamma$  for fixed  $\nu$ , or in the limit of small  $\nu$  for fixed  $\gamma$ , the pseudoscalar terms are suppressed and the NJL<sub>2</sub>

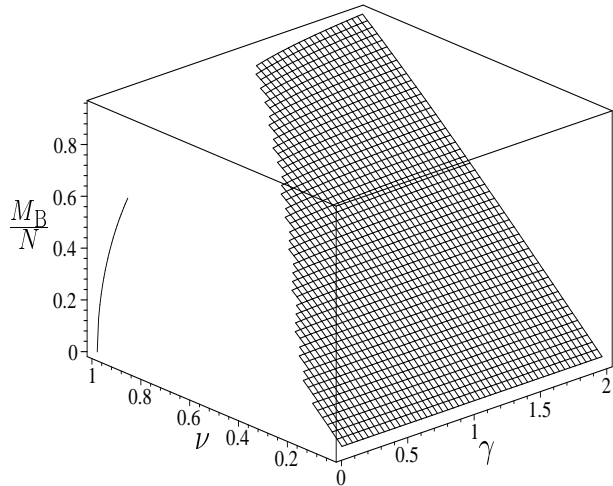


FIG. 3: Analytical results for the baryon mass as a function of filling fraction  $\nu$  and confinement parameter  $\gamma$ . Shown are only results which are stable at the 0.2% level if one removes the highest order correction term. Curve starting at  $\gamma = 0, \nu = 1$ : derivative expansion. Tilted surface: No-sea effective theory.

results converge to those of the GN model. In fact, a non-relativistic approximation to the Dirac equation would be perfectly adequate in this regime. The region where the uppermost filled level reaches the middle of the gap and crosses zero energy lies in the white part of Fig. 3 and has to await a numerical treatment, to which we now turn.

#### IV. NUMERICAL DIRAC-HARTREE-FOCK CALCULATION

##### A. Hamiltonian in discretized momentum space

We first set up the Dirac Hamiltonian in the form of a matrix which can readily be diagonalized numerically. Consider the Hamiltonian

$$H = \gamma_5 \frac{1}{i} \frac{\partial}{\partial x} + \gamma^0 S(x) + i\gamma^1 P(x) \quad (33)$$

with given scalar and pseudoscalar potentials. We choose the representation

$$\gamma^0 = \sigma_1, \quad \gamma^1 = -i\sigma_2, \quad \gamma_5 = \gamma^0\gamma^1 = \sigma_3 \quad (34)$$

of the  $\gamma$  matrices leading to a real symmetric Hamiltonian matrix below. In order to discretize the spectrum of  $H$ , we work in a finite interval of length  $L$  and impose anti-periodic boundary conditions for fermions, resulting in the discrete momenta

$$k_n = \frac{2\pi}{L} \left( n + \frac{1}{2} \right) \quad (n \in \mathbb{Z}). \quad (35)$$

We decompose the potentials into Fourier series,

$$S(x) = \sum_{\ell} S_{\ell} e^{i2\pi\ell x/L}, \quad P(x) = i \sum_{\ell} P_{\ell} e^{i2\pi\ell x/L}. \quad (36)$$

Guided by the analytical results at small and large  $\gamma$  of the preceding sections, we assume that parity is not spontaneously broken in the baryon. A proper choice of the origin in coordinate space then leads to the following symmetry relations for the scalar and pseudoscalar potentials,

$$S(x) = S(-x), \quad P(x) = -P(-x). \quad (37)$$

Together with the reality conditions for  $S$  and  $P$ , we then find that the coefficients  $S_{\ell}, P_{\ell}$  are real and satisfy

$$S_{-\ell} = S_{\ell}, \quad P_{-\ell} = -P_{\ell}, \quad P_0 = 0. \quad (38)$$

The zero mode  $S_0$  of  $S(x)$  acts like a mass term and will be denoted by  $m$  (not to be confused with the physical fermion mass in the vacuum set equal to 1 throughout this paper). We decompose the Hamiltonian as follows,

$$H = H_0 + V, \quad H_0 = \gamma_5 \frac{1}{i} \frac{\partial}{\partial x} + \gamma^0 m, \\ V = \gamma^0 (S(x) - m) + i\gamma^1 P(x), \quad (39)$$

and diagonalize the free, massive Hamiltonian  $H_0$  first,

$$H_0 |\eta, n\rangle = \eta \sqrt{k_n^2 + m^2} |\eta, n\rangle. \quad (40)$$

Here,  $\eta = \pm 1$  is the sign of the energy and  $k_n$  the discrete momentum. The free eigenspinors are given by

$$\langle x | \eta, n \rangle = \frac{1}{\sqrt{2LE}} \begin{pmatrix} \eta \sqrt{E + \eta k} \\ \sqrt{E - \eta k} \end{pmatrix} e^{ikx} \quad (41)$$

with the shorthand notation  $k = k_n, E = \sqrt{k^2 + m^2}$ . Evaluating matrix elements of  $V$  in this basis, we find

$$\langle \eta', n' | V | \eta, n \rangle = \frac{1}{2\sqrt{EE'}} \sum_{\ell \neq 0} \delta_{n-n', \ell} \left( A_{\ell}^{(+)} S_{\ell} + A_{\ell}^{(-)} P_{\ell} \right) \quad (42)$$

( $k' = k_{n'}, E' = \sqrt{(k')^2 + m^2}$ ) with

$$A_{\ell}^{(\pm)} = \eta' \sqrt{E' + \eta' k'} \sqrt{E - \eta k} \pm \eta \sqrt{E + \eta k} \sqrt{E' - \eta' k'}. \quad (43)$$

As  $H_0$  is diagonal, we can now easily construct the full matrix  $\langle \eta', n' | H | \eta, n \rangle$ . We truncate the basis at some momentum index  $\bar{N}$ , keep positive and negative energy states with labels  $-\bar{N} - 1, \dots, \bar{N}$  and diagonalize the resulting  $(4\bar{N} + 4) \times (4\bar{N} + 4)$ -dimensional, real symmetric matrix  $H$  numerically.

##### B. Perturbation theory deep down in the Dirac sea

It is possible and in fact necessary to treat the negative energy states deep down in the Dirac sea perturbatively. First, this restricts the Hamiltonian matrix to be diagonalized numerically to manageable size. Secondly, there is a logarithmic UV divergence in the sum over negative energy states which gets cancelled by a similar divergence

in the double counting correction. This cancellation has to be accomplished analytically before we can hope to reliably extract the finite part. We therefore compute the eigenvalues of  $H$  in 2nd order perturbation theory in  $V$ , in the large volume limit  $L \rightarrow \infty$ . For the negative energy continuum states, we find

$$E_{\text{pert}} = -E(k) - \sum_{\ell=1}^{\ell_{\text{max}}} \frac{E(k)^2 S_{\ell}^2 + k^2 P_{\ell}^2 - 2k_{\ell} E(k) S_{\ell} P_{\ell}}{(k^2 - k_{\ell}^2) E(k)} \quad (44)$$

with  $E(k) = \sqrt{k^2 + m^2}$  and  $k_{\ell} = \pi\ell/L$ . This result is valid for  $k \gg \pi\ell_{\text{max}}/L$ , where the inverse denominators don't blow up. By comparing the perturbative eigenvalues with the ones from diagonalization, we can check whether we have taken into account a sufficient number of basis states and identify any eigenvalues affected by the truncation. The result is an optimal energy  $E_{\text{min}}$ , the energy of the lowest single particle level in the Dirac sea computed by matrix diagonalization.

### C. Computation of the baryon mass

The baryon mass has to be evaluated relative to the vacuum, i.e., as a difference of the HF energies (4) of the baryon and the vacuum. In the NJL<sub>2</sub> model (like in the standard GN model, for that matter) the self-consistent potentials in the vacuum are  $S(x) = 1, P(x) = 0$  in appropriate units. The gap equation (5) serves to eliminate the bare coupling constant from the double counting correction in Eq. (4). For the present discussion it is helpful to split the calculation of the baryon mass into four distinct pieces

$$M_{\text{B}}/N = \Delta E_1 + \Delta E_2 + \Delta E_3 + \Delta E_4 \quad (45)$$

defined as follows. We first evaluate the sum over single particle energies for occupied states resulting from matrix diagonalization (subtracting the vacuum),

$$\Delta E_1 = \sum_{E_{\text{min}}}^{E_{\text{max}}} (E_{\alpha} - E_{\alpha}^{\text{vac}}). \quad (46)$$

$E_{\text{min}}$  has been introduced before,  $E_{\text{max}}$  denotes the energy of the highest occupied level in the baryon. The vacuum single particle energies  $E_{\alpha}^{\text{vac}}$  are computed in a finite interval (length  $L$ ) from the free massive theory with  $m = 1$ . Next we decompose the perturbative single particle energies (44) according to their UV behavior,

$$E_{\text{pert}} = -E(k) - \sum_{\ell=1}^{\ell_{\text{max}}} \frac{S_{\ell}^2 + P_{\ell}^2}{E(k)} - \sum_{\ell=1}^{\ell_{\text{max}}} \frac{E(k_{\ell})^2 S_{\ell}^2 + k_{\ell}^2 P_{\ell}^2 - 2k_{\ell} E(k) S_{\ell} P_{\ell}}{(k^2 - k_{\ell}^2) E(k)}. \quad (47)$$

The last term on the right-hand side behaves asymptotically like  $1/k^2$  and can be integrated over momenta without cutoff. The resulting convergent integral defines the

contribution  $\Delta E_2$  to the baryon mass,

$$\Delta E_2 = -2L \int_{k_{\text{min}}}^{\infty} \frac{dk}{2\pi} \sum_{\ell=1}^{\ell_{\text{max}}} \frac{E(k_{\ell})^2 S_{\ell}^2 + k_{\ell}^2 P_{\ell}^2 - 2k_{\ell} E(k) S_{\ell} P_{\ell}}{(k^2 - k_{\ell}^2) E(k)} \quad (48)$$

and can be computed analytically ( $k_{\text{min}}$  is determined by  $E_{\text{min}}$  introduced above). The first two terms in Eq. (47), after vacuum subtraction, give rise to an elementary, logarithmically divergent integral which has to be regularized with the same cutoff as the gap equation and will be denoted by  $\Delta E_3$ ,

$$\begin{aligned} \Delta E_3 &= -2L \int_{k_{\text{min}}}^{\Lambda/2} \frac{dk}{2\pi} \left( E(k) + \sum_{\ell=1}^{\ell_{\text{max}}} \frac{S_{\ell}^2 + P_{\ell}^2}{E(k)} \right. \\ &\quad \left. - \sqrt{k^2 + 1} \right) \\ &= -\frac{L}{2\pi} \left( m^2 - 1 + 2 \sum_{\ell=1}^{\ell_{\text{max}}} (S_{\ell}^2 + P_{\ell}^2) \right) \ln \Lambda + \Delta \tilde{E}_3. \end{aligned} \quad (49)$$

$\Delta \tilde{E}_3$  is the finite part which can again be computed analytically. Finally,  $\Delta E_4$  is the (vacuum subtracted) double counting correction,

$$\begin{aligned} \Delta E_4 &= \frac{L}{2\pi} \left( m^2 - 1 + 2 \sum_{\ell=1}^{\ell_{\text{max}}} (S_{\ell}^2 + P_{\ell}^2) \right) (\gamma + \ln \Lambda) \\ &\quad - \frac{\gamma L}{\pi} (m - 1). \end{aligned} \quad (50)$$

In the sum  $\Delta E_3 + \Delta E_4$  the  $\ln \Lambda$  terms are cancelled exactly and a finite result for  $M_{\text{B}}/N$ , Eq. (45), is obtained.

### D. Finding the self-consistent potential

In non-relativistic HF calculations, one usually determines the self-consistent potential iteratively. Starting from some guess, one solves the HF equation, computes the new HF potential and repeats this procedure until it has converged. This method was also employed in Ref. [9] for the 't Hooft model, using a lattice discretization in coordinate space. We do not have this option here. The reason is the fact that we work in the continuum and have already sent the UV cutoff to  $\infty$  and the bare coupling constant to 0. As is clear from the self-consistency relations (3), in this case the HF potential is determined by the far UV region where lowest order perturbation theory holds. Therefore we always get back the potential which we put in, irrespective of what we choose. If we would keep the cutoff finite like on the lattice, we could in principle use an iteration, but the convergence would slow down with increasing cutoff. A way out of this problem was found in Ref. [23] for the GN model where the HF energy of the baryon was simply minimized with respect to the potential  $S(x)$ . Technically, the minimization was done with respect to the Fourier coefficients  $S_{\ell}$  of  $S(x)$ . In the NJL<sub>2</sub> case there are twice as many parameters due

to the pseudoscalar potential, so that this method would be rather cumbersome. Moreover, owing to the analytical calculations in Secs. II and III, we already have a fairly good qualitative idea of how the potentials should look like. Hence the following strategy has turned out to be more economic. We write down a parametrization of  $S$  and  $P$  which is both flexible and well suited to the known limiting cases. We then vary with respect to the parameters. Since we are only interested in a limited precision, a relatively small number of parameters is sufficient, provided the parametrization is judiciously chosen. The convergence can be checked by comparing runs with different numbers of parameters. A natural ansatz for trial functions in the present problem is given by

$$S(x) = \sum_{k=1}^K \frac{c_k}{\cosh^{2k} \xi}, \quad P(x) = \sum_{k=1}^K \frac{d_k \sinh \xi}{\cosh^{2k+1} \xi} \quad (51)$$

( $\xi = yx$ ). This is clearly compatible with the no-sea effective theory, see Eq. (22). The derivative expansion would suggest even powers of  $1/\cosh \xi$  in  $P(x)$  at low  $\gamma$  rather than odd powers, see Eq. (10), but this makes almost no difference in practice, once we keep a sufficient number of terms. The coefficients  $c_k, d_k$  and the scale parameter  $y$  serve as variational parameters. The baryon mass computed as explained above is a function of these parameters and is minimized in the  $(2K+1)$ -dimensional parameter space via some standard algorithm.

### E. Numerical results

All the results shown below were obtained by keeping the first three terms in each sum, Eq. (51), and varying with respect to 6 coefficients ( $c_k, d_k$ ) and the scale parameter  $y$ . We found that a matrix dimension  $804 \times 804$  (corresponding to  $\bar{N} = 200$  in Sec. IV A) and box size  $L = 20$  (in units where  $m = 1$ ) were adequate. The minimum in the 7-dimensional space was found with a standard conjugate gradient method involving 70 iteration steps. We first tested the whole procedure for several values of  $\nu, \gamma$  where the analytical approaches are expected to be reliable. For example, at  $\gamma = 0.2, \nu = 1$  the derivative expansion gives  $M_B = 0.52227$  and the numerical HF calculation  $M_B = 0.52248$ . This is satisfactory, especially since the numerical value is the result of subtracting large numbers (of the order of 10 000) due to the Dirac sea, cf. Eq. (46). The scalar and pseudoscalar HF potentials are indistinguishable on a plot if one compares the derivative expansion with the full HF calculation, therefore we don't show them here. At  $\gamma = 5.0, \nu = 1$  the no-sea effective theory yields  $M_B = 0.98847$  as compared to the numerical HF calculation  $M_B = 0.98850$ , again with excellent agreement of the self-consistent potentials. We also tested the HF calculation against the no-sea effective theory at small filling. For  $\gamma = 0.2, \nu = 0.2$  the analytical value  $M_B = 0.197314$  compares well with the

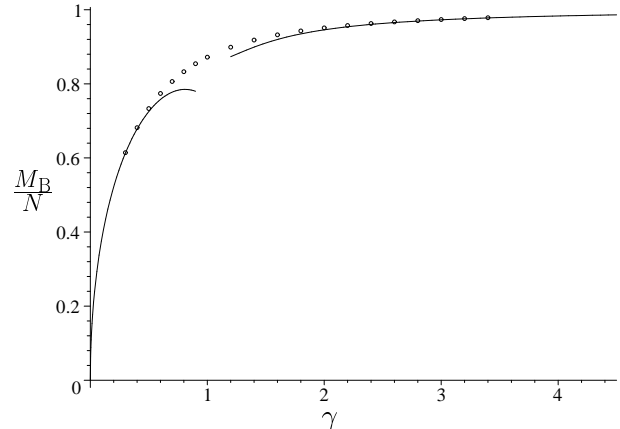


FIG. 4: Circles: numerical results for baryon mass at  $\nu = 1$  versus  $\gamma$ . Curves: analytical asymptotic predictions (derivative expansion to the left, no-sea effective theory to the right).

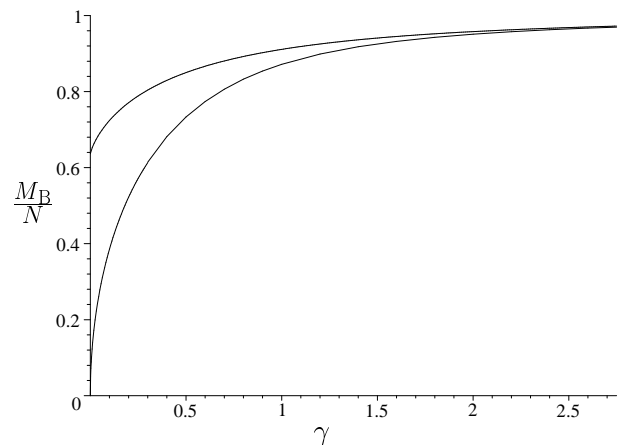


FIG. 5: Comparison of baryon mass for large  $N$  GN (upper curve) and  $NJL_2$  (lower curve) models, at  $\nu = 1$ . These curves can be regarded equally well as zero temperature phase boundaries in the  $(\mu, \gamma)$ -plane.

numerical result  $M_B = 0.197337$ . These examples give strong support to the numerical method as well as to the (independent) analytical calculations.

Regarding the phase diagram, the question of most immediate interest is the dependence of  $M_B$  on  $\gamma$  for full occupation  $\nu = 1$ . This is expected to yield a critical (2nd order) curve in the phase diagram at  $T = 0$ . In Fig. 4 we show the numerical points together with the asymptotic expansions, using both derivative expansion and no-sea effective theory. In Fig. 5 we compare this newly calculated baryon mass in the massive  $NJL_2$  model with the known one from the massive GN model, choosing a somewhat smaller range of  $\gamma$  as compared to Fig. 4 to highlight the differences. The two curves shown reflect directly the critical lines in the  $(\mu, \gamma)$ -plane at  $T = 0$  of the respective phase diagrams. As a by-product of the calculation of baryon masses we also get the single particle energy

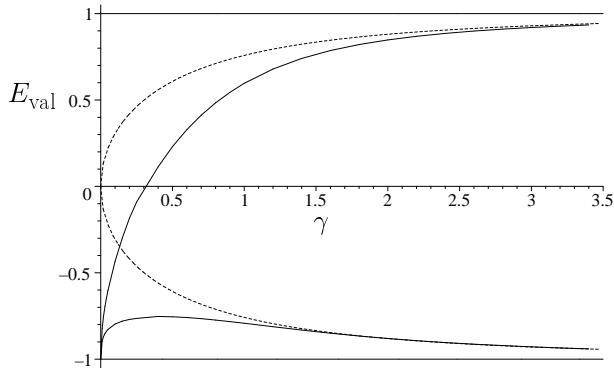


FIG. 6: Energies of valence levels for GN model (dashed curves) and  $\text{NJL}_2$  model (solid curves) versus  $\gamma$ , illustrating how the  $\text{NJL}_2$  baryon interpolates between a Skyrme-type baryon with induced fermion number and a conventional, non-relativistic, valence-type baryon.

of the valence levels, i.e., discrete levels inside the mass gap. It is instructive to compare these energies between the GN and  $\text{NJL}_2$  models as well. Fig. 6 shows the pair of (charge conjugation) symmetric states in the GN model which come together at zero energy at  $\gamma = 0$  (this point corresponds to a kink and antikink at infinite separation). The baryons in the  $\text{NJL}_2$  model also feature a pair of discrete states which approach those of the GN model at large  $\gamma$ . At small  $\gamma$ , they converge to the lower edge of the mass gap, the upper level crossing zero near  $\gamma_0 = 0.3$ . Both of these valence levels are fully occupied. Below  $\gamma_0$  one would talk about induced fermion number (the number of negative energy levels changes as compared to the vacuum), whereas above  $\gamma_0$  one has ordinary valence fermions like in the GN model. Note however that nothing discontinuous happens at the “spectral flow” point  $\gamma_0$ . This picture nicely illustrates the transition from the massless baryon at  $\gamma = 0$  (with baryon number given by winding number of the pion field, like in the Skyrmin case) to the weakly bound non-relativistic baryon emerging at large  $\gamma$  in either GN or  $\text{NJL}_2$  models. The latter one is apparently insensitive to the original type of chiral symmetry, be it  $U(1)$  or  $Z_2$ .

The HF potentials belonging to these calculations are shown in Figs. 7-10. Fig. 7 is a 3d-plot containing the full information how  $S$  and  $P$  depend on  $x$  for 20 different values of  $\gamma$ . The 3 different projections of this plot onto the coordinate planes show the  $x$ -dependence of  $S$  (Fig. 8) and  $P$  (Fig. 9) in more detail, as well as parametric contour plots in the  $(S, P)$ -plane (Fig. 10). We can infer from this last figure that the chiral winding number jumps from 1 to 0 slightly below  $\gamma = 0.7$ , where the contour plot hits the origin (close to the 5th curve from the outside). Note that this does not coincide with the value  $\gamma_0 = 0.3$  where the upper valence level crosses zero, so that induced fermion number is not directly related to winding number of  $\Phi = S - iP$  for larger bare fermion masses. This is in agreement with the general observa-

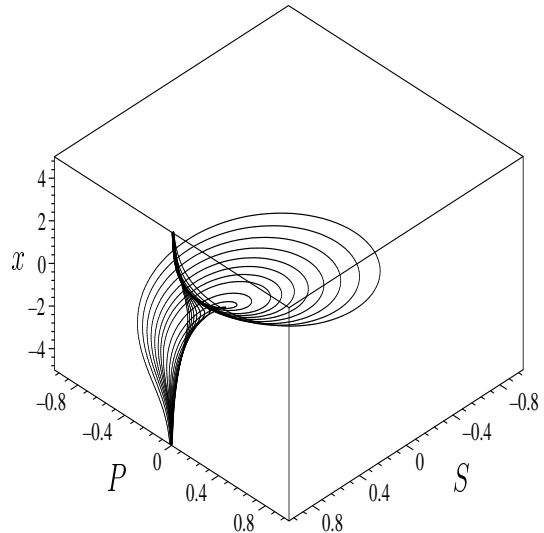


FIG. 7: HF potentials  $S, P$  versus  $x$  in a 3d plot. The curves correspond to  $\gamma = 0.3, \dots, 1.0$  in steps of 0.1 and  $\gamma = 1.2, \dots, 3.4$  in steps of 0.2. The outermost curve has the smallest value of  $\gamma$ . The curves at large  $\gamma$  accumulate around  $S = 1, P = 0$  and are not well resolved, see also Figs. 8–10

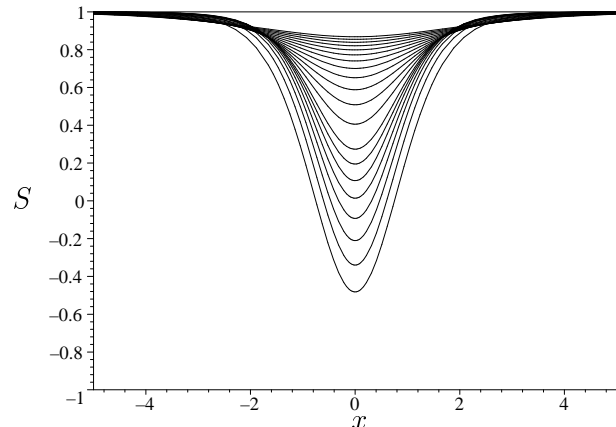


FIG. 8: Projection of Fig. 7 onto the  $(x, S)$ -plane, showing how the shape of the scalar potential evolves with  $\gamma$ .

tion that the integer part of induced fermion number is not topological, being sensitive to spectral flow [24].

Although it is presumably not relevant for the phase diagram, we now turn to baryons with partially occupied valence level. The HF calculation can be done exactly as before, except that the single particle energy of the upper valence level is weighted by the occupation fraction  $\nu$  when calculating the baryon mass. We have carried out detailed studies of the  $\nu$ -dependence for the three values  $\gamma = 0.2, 0.6, 1.0$  and compared the HF results with the no-sea effective theory expected to describe correctly the  $\nu \rightarrow 0$  behavior. The results for the baryon mass are shown in Figs. 11-13 and again underline the value of the much simpler analytical results.

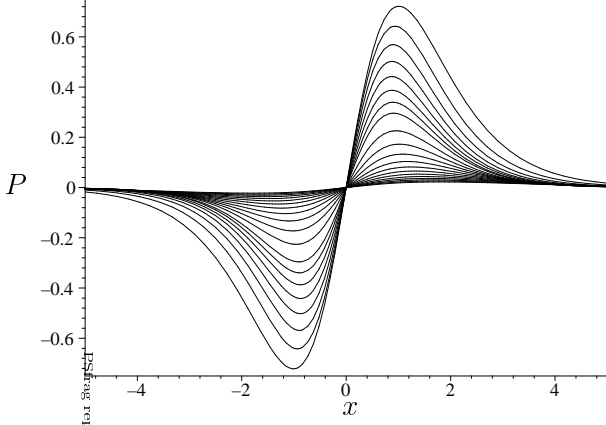


FIG. 9: Analogous to Fig. 8, but for the  $(x, P)$ -plane and pseudoscalar potential.

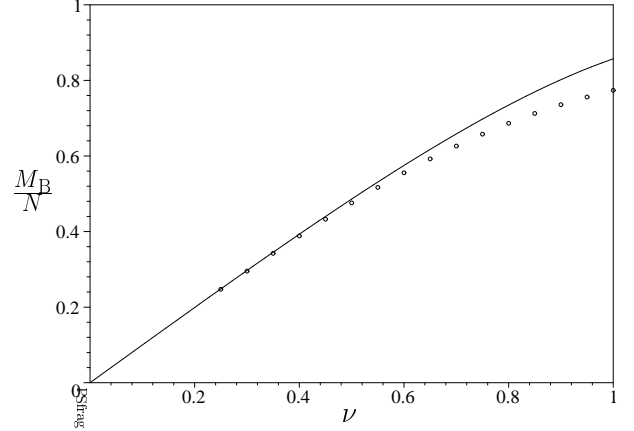


FIG. 12: Same as Fig. 11, but for  $\gamma = 0.6$ .

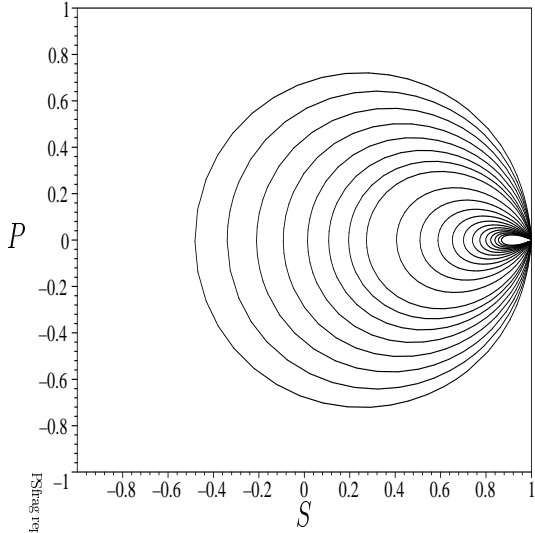


FIG. 10: Projection of Fig. 7 onto the  $(S, P)$ -plane.

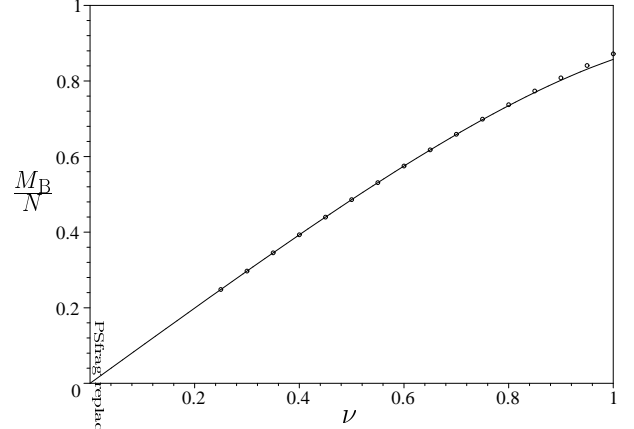


FIG. 13: Same as Fig. 11, but for  $\gamma = 1.0$ .

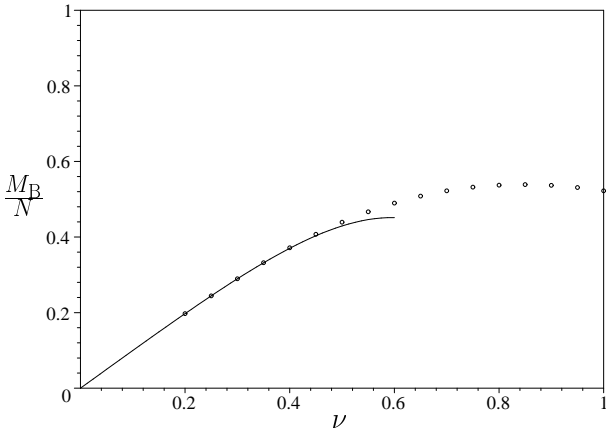


FIG. 11: Baryon mass in the NJL<sub>2</sub> model versus filling fraction  $\nu$  of upper valence level, for  $\gamma = 0.2$ . Circles: numerical HF calculation, curve: analytical prediction based on the non-sea effective theory.

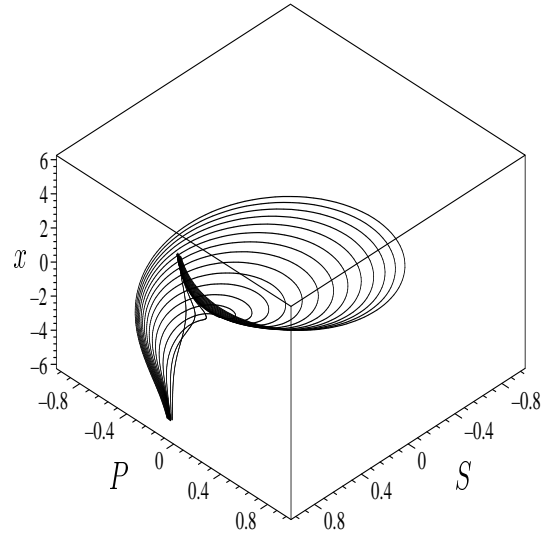


FIG. 14: HF potentials  $S, P$  versus  $x$  in a 3d plot. The 17 curves correspond to  $\nu = 0.2, \dots, 1.0$  in steps of 0.05. The outermost curve has the largest value of  $\nu$ .

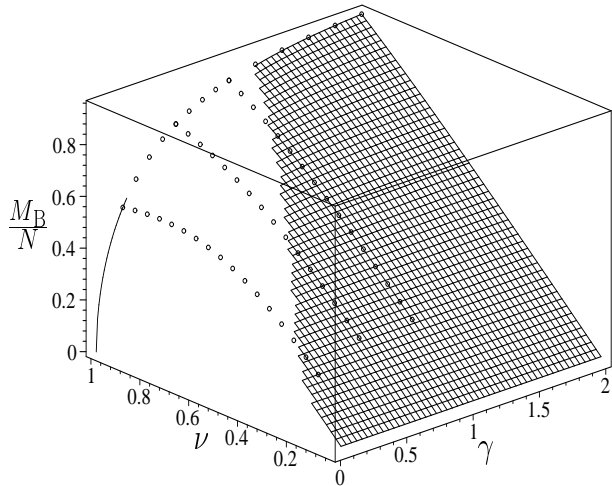


FIG. 15: Baryon mass as a function of filling fraction  $\nu$  and confinement parameter  $\gamma$ . The numerical HF results (circles) have been combined with the analytical results of Fig. 3, completing the picture of what is known by now.

The self-consistent potentials as a function of  $\nu$  are illustrated for the case  $\gamma = 0.2$  in Fig. 14 (the other cases are qualitatively similar). This 3d-plot corresponds to Fig. 7, except that now the different curves are obtained by varying  $\nu$  at fixed  $\gamma$  rather than  $\gamma$  at fixed  $\nu$ . The similarity between Figs. 7 and 14 is quite remarkable. Depleting the valence level has apparently a very similar effect as increasing the bare fermion mass, i.e., it drives the NJL<sub>2</sub> baryon into the non-relativistic regime where it becomes indistinguishable from the GN baryon.

In order to summarize the results obtained in the present work, we have combined all the available points from the numerical HF calculations with the analytical results taken from Fig. 3, see Fig. 15. The numerical points start to fill the white gap in Fig. 3 and match perfectly onto the analytical predictions in the region where these can be trusted. This can be seen more clearly in the 2d-plots of Figs. 4 and Figs. 11–13. We do not show any results for  $\gamma > 2$  where the asymptotic formula (31) is fully adequate. Notice that when the present work was started, only the short solid curve starting at  $\nu = 1, \gamma = 0$  had been known from the derivative expansion [12].

## V. SUMMARY AND CONCLUSIONS

This paper is part of an ongoing effort to establish the phase diagram of (large  $N$ ) Gross-Neveu type models. Ultimately, we would like to construct the phase diagram of the massive NJL<sub>2</sub> model in  $(\gamma, \mu, T)$  space in a similarly complete fashion as what has already been achieved for the massive GN model. One important building block which was still missing are the baryons in the massive NJL<sub>2</sub> model. The only source of information so far was the derivative expansion, restricted to the vicinity of the

chiral limit and to completely filled single particle levels. After briefly reviewing these results, we have identified another parameter region where systematic analytical approximations can be performed, namely the non-relativistic regime (heavy fermions or weak filling of the valence level). Here, a recently developed no-sea effective theory has proven to be very efficient. The gap between these two asymptotic approaches could only be filled at the expense of full numerical HF calculations including the Dirac sea. As a result, we have obtained a rather comprehensive picture of how the baryon evolves from a Skyrme-type topological object in the chiral limit to a non-relativistic valence bound state. The transition from induced fermion number to valence fermion number has a simple interpretation in terms of spectral flow as a function of the confinement parameter, as discussed in connection with Fig. 6. In the heavy fermion limit, it becomes irrelevant whether the model had originally a U(1) or Z<sub>2</sub> chiral symmetry, and the results for the massive NJL<sub>2</sub> and GN models converge.

As compared to the massive GN model with its complete analytical solution, the analysis of the massive NJL<sub>2</sub> model is significantly more involved. Although the self-consistent potentials which we find numerically appear to have simple shapes, we have not been able to come up with an analytical solution. One source of difficulty is the fact that the potentials in the NJL<sub>2</sub> model are not reflectionless. Related to this, even in those limits where we have analytical control, the potentials do not lead to any known exactly solvable Dirac equation. If this problem is analytically tractable at all, the techniques must be quite different from those which have been successful in the GN model case.

Finally, coming back to the phase diagram, we have in fact determined one particular phase boundary in the present work. Like in the GN model, the  $T = 0$  base line of the phase diagram in  $(\gamma, \mu, T)$  space is expected to be given by the curve  $M_B(\gamma)$  of Figs. 4 and 5. Another piece of information about the phase diagram is the vicinity of the tricritical point discussed recently in Ref. [25]. To complete this picture remains quite a challenge.

### APPENDIX A: RESULTS FOR COEFFICIENTS DEFINED IN SEC. III

Here we collect the  $\gamma$ -dependent coefficients which enter the results of the no-sea effective theory in Sec. III. Coefficients for the scalar potential  $S$ , Eq. (22),

$$\begin{aligned}
s_{22} &= -\frac{1}{4(1+\gamma)^2}, & s_{42} &= \frac{5\gamma^2 + 3\gamma + 2}{96\gamma(1+\gamma)^5} \\
s_{44} &= -\frac{3\gamma + 4}{64\gamma(1+\gamma)^4} \\
s_{62} &= -\frac{91\gamma^4 - 102\gamma^3 + 275\gamma^2 + 276\gamma + 88}{23040\gamma^2(1+\gamma)^8} \\
s_{64} &= \frac{81\gamma^3 + 13\gamma^2 - 140\gamma - 24}{9216\gamma^2(1+\gamma)^7} \\
s_{66} &= -\frac{45\gamma^2 - 136\gamma - 60}{9216\gamma^2(1+\gamma)^6} \tag{A1}
\end{aligned}$$

Coefficients for the pseudoscalar potential  $P$ , Eq. (22),

$$\begin{aligned}
p_{33} &= \frac{1}{8\gamma(1+\gamma)^2}, & p_{53} &= -\frac{(3\gamma + 2)(\gamma - 3)}{192\gamma^2(1+\gamma)^5} \\
p_{55} &= \frac{\gamma - 2}{64\gamma^2(1+\gamma)^4} \tag{A2}
\end{aligned}$$

Coefficients for the valence fermion density  $\rho_{\text{val}}$ , Eq. (28),

$$\begin{aligned}
v_{22} &= \frac{1}{4(1+\gamma)}, & v_{42} &= -\frac{\gamma^2 + \gamma + 1}{48\gamma(1+\gamma)^4} \\
v_{44} &= \frac{\gamma + 4}{64\gamma(1+\gamma)^3} \\
v_{62} &= \frac{2\gamma^4 + 10\gamma^3 + 49\gamma^2 + 37\gamma + 11}{2880\gamma^2(1+\gamma)^7} \\
v_{64} &= -\frac{15\gamma^3 + 151\gamma^2 + 76\gamma + 48}{9216\gamma^2(1+\gamma)^6} \\
v_{66} &= \frac{9\gamma^2 - 40\gamma + 12}{9216\gamma^2(1+\gamma)^5} \tag{A3}
\end{aligned}$$

Coefficients for the induced fermion density  $\rho_{\text{ind}}$ , Eq. (29),

$$\begin{aligned}
i_{42} &= \frac{1}{16\gamma(1+\gamma)^3}, & i_{44} &= -\frac{3}{32\gamma(1+\gamma)^3} \\
i_{62} &= -\frac{2\gamma^2 - 5\gamma - 4}{192\gamma^2(1+\gamma)^6}, & i_{64} &= \frac{4\gamma^2 - 7\gamma - 8}{128\gamma^2(1+\gamma)^6} \\
i_{66} &= -\frac{5(\gamma - 2)}{256\gamma^2(1+\gamma)^5} \tag{A4}
\end{aligned}$$

- 
- [1] D. J. Gross and A. Neveu, Phys. Rev. D **10**, 3235 (1974).  
[2] U. Wolff, Phys. Lett. B **157**, 303 (1985).  
[3] A. Barducci, R. Casalbuoni, M. Modugno, G. Pettini, and R. Gatto, Phys. Rev. D **51**, 3042 (1995).  
[4] M. Thies, J. Phys. A: Math. Gen. **39**, 12707 (2006).  
[5] R. F. Dashen, B. Hasslacher, and A. Neveu, Phys. Rev. D **12**, 2443 (1975).  
[6] Y. Nambu and G. Jona-Lasinio, Phys. Rev. **122**, 345 (1960); *ibid.* **124**, 246 (1961).  
[7] V. Schön and M. Thies, Phys. Rev. D **62**, 096002 (2000).  
[8] F. Karbstein and M. Thies, Phys. Rev. D **76**, 085009 (2007).  
[9] L. L. Salcedo, S. Levit and J. W. Negele, Nucl. Phys. B **361**, 585 (1991).  
[10] G. 't Hooft, Nucl. Phys. B **75**, 461 (1974).  
[11] T. H. R. Skyrme, Proc. Roy. Soc. London A **260**, 127 (1961).  
[12] M. Thies and K. Urlichs, Phys. Rev. D **71**, 105008 (2005).  
[13] E. Witten, Nucl. Phys. B **160**, 57 (1979).  
[14] S.A. Brazovskii and N.N. Kirova, JETP Lett. **33**, 4 (1981).  
[15] J. Feinberg and A. Zee, Phys. Lett. B **411**, 134 (1997).  
[16] F. Karbstein and M. Thies, Phys. Rev. D **77**, 025008 (2008).  
[17] I.J.R. Aitchison and C.M. Fraser, Phys. Rev. D **31**, 2605 (1985).  
[18] G.V. Dunne, J. Lopez-Sarrion, and K. Rao, Phys. Rev. D **66**, 025004 (2002).  
[19] K. Urlichs, phd thesis, Erlangen (2006).  
[20] J. Feinberg, Ann. Phys. **309**, 166 (2004).  
[21] J. Feinberg and A. Zee, Int. J. Mod. Phys. A **12**, 1133 (1997).  
[22] J. Feinberg and A. Zee, in: M. Olshanetsky and A. Vainshtein, (eds.), *Multiple facets of quantization and supersymmetry*, World Scientific, p. 626 (2002).  
[23] M. Thies and K. Urlichs, Phys. Rev. D **67**, 125015 (2003).  
[24] A.J. Niemi and G.W. Semenoff, Phys. Rep. **135**, 99 (1986).  
[25] C. Boehmer, M. Thies and K. Urlichs, Phys. Rev. D **75**, 105017 (2007).